Magnetic induction tomography: resolution and penetrating power through metal shields

B. Darrer[a], P. Bartlett[a], J. Watson[b], F. Renzoni[a]

[a]Department of Physics and Astronomy, University College London, Gower Street, London, WC1E 6BT, United Kingdom
[b]Atomic Weapons Establishment, Aldermaston, Reading, RG7 4PR, United Kingdom

Abstract

Magnetic induction tomography (MIT) is a non-contact imaging technique that has applications in security, industry and medicine. The resolution of a MIT system was investigated, as was the system's ability to image metallic objects through metal shields. The technique employs a driver-coil and sensor-coil. The sample object was imaged via phase-variance measurements between the two coils, due to inductive coupling between the coils and the sample object. The resolution of the MIT system was investigated by producing images of different arrangements of steel ball-bearings. The penetrating power was also demonstrated by imaging a mild-steel bar through a ferromagnetic shield.

Keywords: Magnetic Induction Tomography (MIT); eddy currents; imaging; resolution; alternating magnetic-field; metal shield

1. Introduction

Magnetic induction tomography (MIT) [1-10] is a non-contact electromagnetic imaging technique that has potential applications in security, industry and medicine. MIT has been the object of intensive research in the context of biomedical applications, but it is not yet a well-developed tool for imaging metallic objects and has barely been researched for imaging through metal shields.

In MIT a driver coil produces an alternating magnetic-field (primary field), that induces eddy currents in the sample object, producing a secondary opposing magnetic-field. This secondary field is indirectly measured by the sensor coil [3] [5]. The changes in phase difference between the driver and sensor coil potential-differences are due to the sample object's electromagnetic properties: conductivity, permeability and permittivity [4-6].

In this study the measurement of the phase difference between the two coils is used to image a sample object in two dimensions. This is done by moving the sample with respect to the common axis of the coils. The resolution of the MIT system was investigated by producing images of different arrangements of steel ball-bearings. The penetrating power of the system was also demonstrated by imaging steel ball-bearings and a mild-steel bar through metal shields.

2. Experimental set-up

A lock-in amplifier measures the potential difference (p.d.) induced across the sensor coil with respect to the reference p.d. applied across the driver coil. When the sample is placed between the coils, the magnitude and phase of the sensor coil's p.d. change. This is due to the additional magnetic field generated by the eddy currents induced in the sample object by the primary field [11] [3].

Our apparatus consists of a driver coil and a sensor coil, with external diameters (12.4 ± 0.1) cm and (6.90 ± 0.03) mm respectively; the sensor coil being a commercially available inductor of 680 µH. The sensor-coil axis is collinear with the driver coil one. The coils are placed on a Perspex rig to magnetically isolate the experiment. The sensor coil being attached to the underside of the lower platform. The sample object (e.g. a steel ball-bearing) was placed on a slider which could be moved in the plane perpendicular to the coils axis, and whose position could be determined with an accuracy of 1 mm.

Typical AC magnetic flux densities for our setup are as follows: The RMS magnetic flux density, level with the bottom of the driver coil and at its centre, was measured as; (2.51 ± 0.01) mT at 500 Hz and 27.2 V RMS

across driver coil; (0.170 ± 0.003) mT at 5 kHz and 27 V RMS; (0.197 ± 0.002) mT at 5 kHz and 31 V RMS. The RMS magnetic flux density at the level of the sensor coil was measured as; (0.76 ± 0.03) mT at 500 Hz and 27.2 V RMS across driver coil; (0.042 ± 0.003) mT at 5 kHz and 27 V RMS; (0.060 ± 0.005) mT at 5 kHz and 31 V RMS.

For a given position of the sample object, the phase difference between the p.d. across the driver coil and that of the sensor coil was measured with a Signal Recovery 7230 DSP lock-in amplifier. Firstly, a 150W AC amplifier supplies an AC signal at 27 V for most of the experiments and 31 V for imaging through ferromagnetic and Aluminium-foil shields. A digital oscilloscope was used to monitor the signals in both coils, also generating a Lissajous figure to give a visual display of the p.d. phase-difference changing as the metallic sample is moved between the coils. A second oscilloscope was used to directly monitor the AC p.d. across the driver coil, as the digital oscilloscope only monitors the driver-coil p.d. before amplification. AC frequencies applied across the driver coil in this study were 500 Hz, 5 kHz, 10 kHz and 20 kHz.

3. Experimental results and discussion

3.1 MIT of steel ball-bearings in various arrangements

In order to estimate the resolving power of our MIT system, we imaged several steel ball-bearings of different diameters, either individually or arranged as different 1D and 2D planar structures.
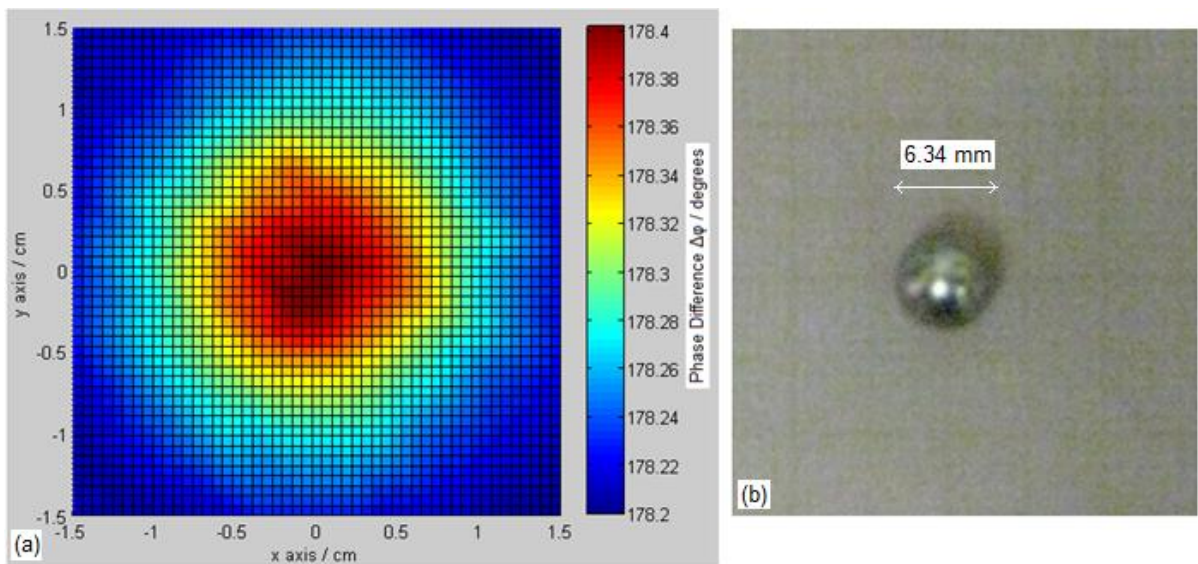

Fig. 1. (a) 2D MIT surface plot of a 6.34 mm diameter steel ball-bearing. The plot was created from 121 (x, y, phase) measurements. (b) Photograph of the ball bearing is to approximate scale with the plot.
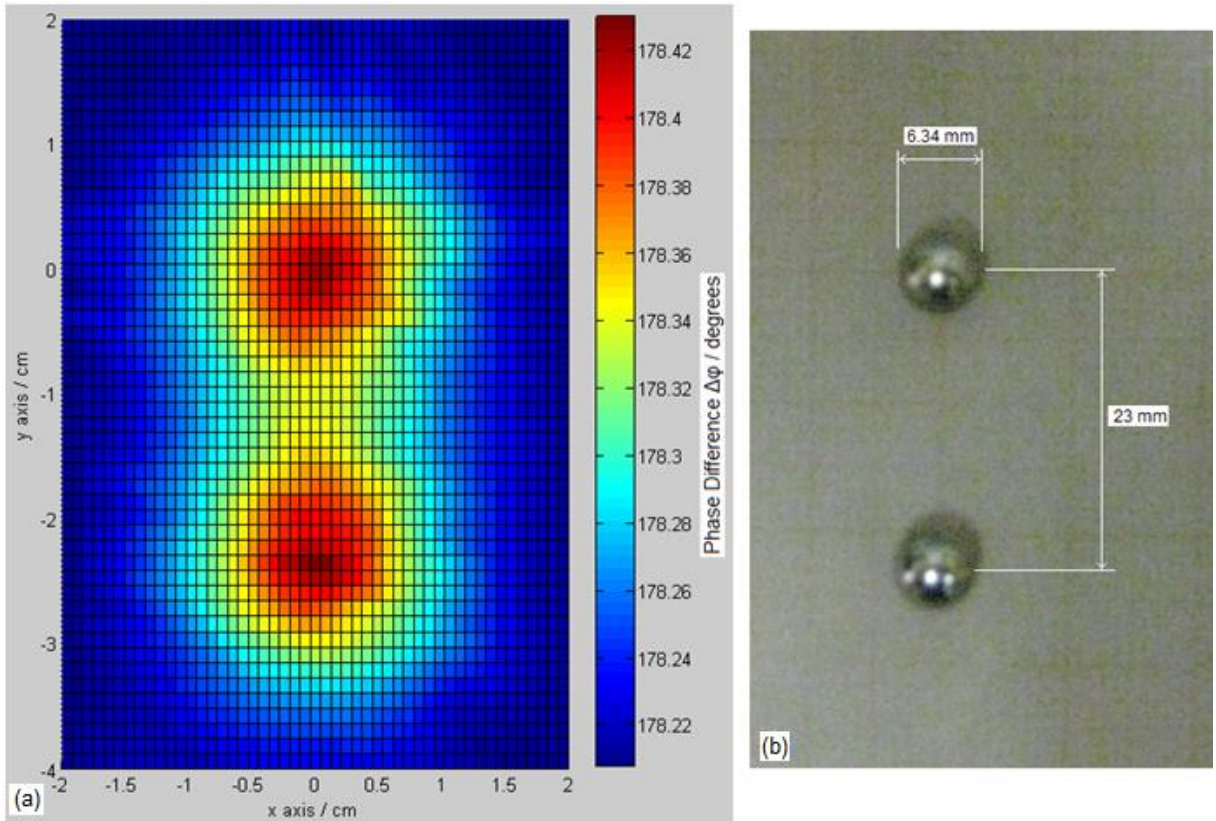
Fig. 2. (a) 2D MIT surface plot of a 2 × 6.34 mm diameter steel ball-bearings separated by 2.3 cm.
The plot was created from 261 (*x*, *y*, phase) measurements. (b) Photograph of ball bearings is to approximate scale with the plot.
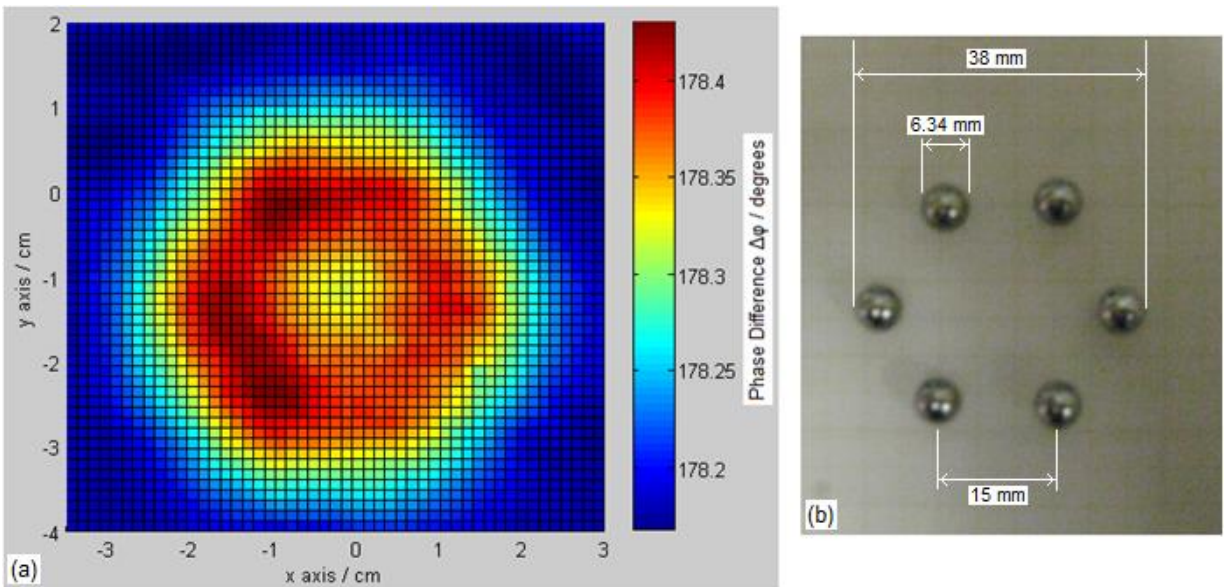

Fig. 3. (a) 2D MIT surface plot of 6 × 6.34 mm diameter steel ball-bearings arranged as a hexagon.
The plot was created from 455 (*x*, *y*, phase) measurements. (b) Photograph of the hexagon is to approximate scale with the plot.

Two dimensional MIT images were produced by moving the metallic object in steps in the *x* and *y* directions, and by taking one phase measurement for each position. Figures 1, 2 and 3 show the 2D surface plots of 6.34 mm diameter steel ball-bearings in various arrangements. Figure 1 reports the MIT image of a single ball bearing.

The arrangement of two ball bearings separated by a distance of 2.3 cm is used for the measurements reported in Figure 2. Those measurements clearly demonstrated that the two ball-bearings can be clearly resolved, thus providing an indication that the resolving power of MIT system is at least 23 mm. Additional measurements were performed for six ball bearings arranged as an hexagon of side 15 mm. Figure 3 shows that while the hexagon shape can be clearly identified, the individual ball bearing cannot be resolved. Thus the combination of the results of figures 2 and 3 give a resolving power of our system between 15 and 23 mm.

3.2 Measurement of object's diameter via MIT

Another simple approach to investigate the resolving power of the MIT system is via the measurement of the diameter of ball bearings. We used our MIT apparatus to produce 1D plots of individual ball bearings of different dimensions. From each measurement we derived the diameter of the ball bearing as the full width at half maximum (FWHM) of the image in a 1D phase-difference plot. This was based on the assumption that the symmetric 1D phase-difference images of circular metallic-objects were close to a Gaussian shaped curve, and that the diameter may be determined via the FWHM values. Besides the ball bearings, we also examined British 1 pence and a set of two 2 pence coins on top of each other. The results of our measurements are summarized in figure 4, where for the different objects the diameter measured via MIT is plotted against the actual diameter, as measured with a micrometer. The figure includes three steel ball-bearings of different sizes - diameters: 6.34 mm, 3.17 mm and 2.77 mm, at 3 frequencies (5 kHz, 10 kHz, 20 kHz) and two bronze coins (1 × one pence and 2 × two pence) imaged at 500 Hz.

The images of one and two pence coins (pre-1992 coins, each made of bronze: 97% copper, 2.5% zinc, 0.5% tin) showed that FWHM gave a close correlation with 'true' diameter for the 2 × two pence coins (FWHM = (26.1 ± 0.7) mm, diameter = 26 mm) and the one pence coin of 20 mm diameter gave FWHM = (25.7 ± 0.3) mm (see figures 4 and 5). For smaller metallic objects, such as the ball bearings, the maximum p.d. phase-difference is much lower than with the coins, so with less phase-difference data in their 1D
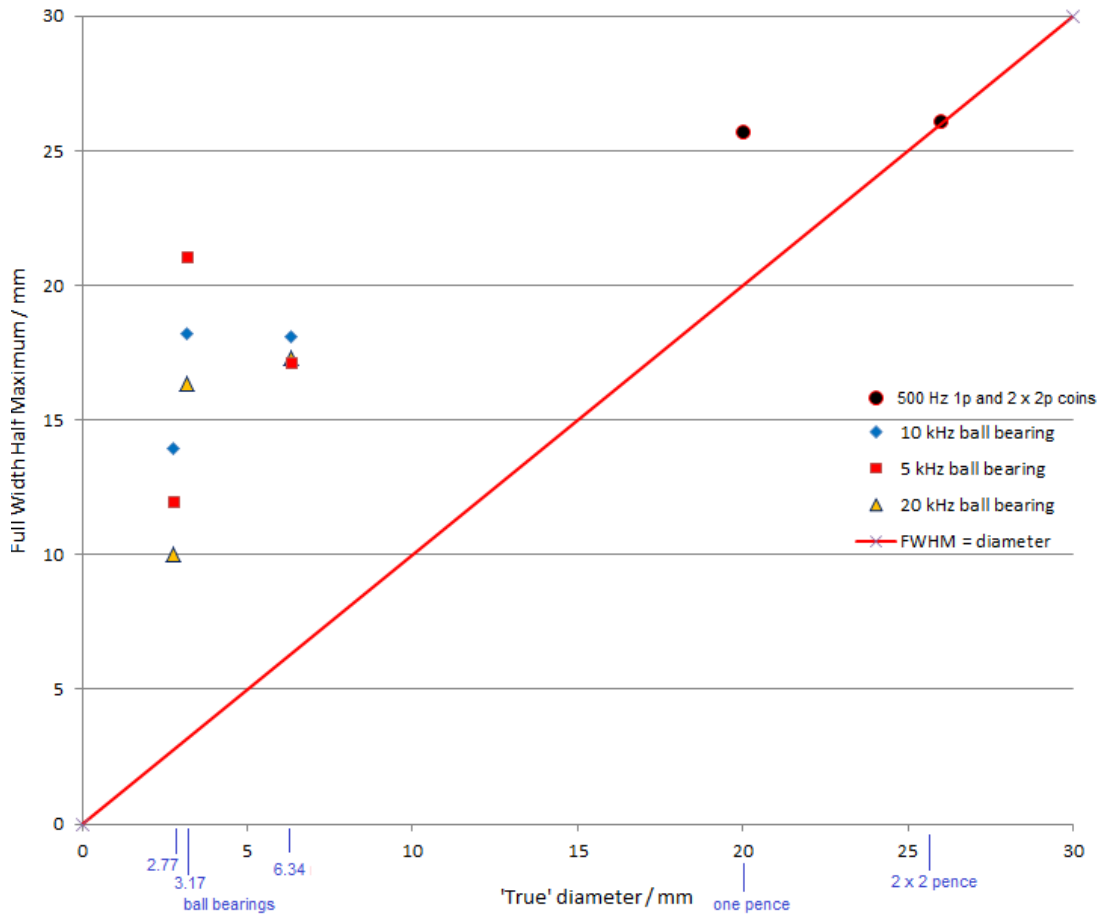
Fig. 4. Scatter Plot showing Full Width at Half Maximum (FWHM) against 'true' diameter of 3 sizes of steel ball bearings (diameters: 6.34 mm, 3.17 mm, 2.77 mm), measured with micrometer. The FWHM is taken from 1D image plots of each ball bearing at AC frequencies 5 kHz, 10 kHz and 20 kHz with 27.0 V (RMS) applied across the driver coil in each case. Note: The 1.98 mm diameter ball bearing gave zero phase differences at 5 kHz and was also considered a null result at 10 kHz and 20 kHz, and has not been included in the above plot. The plot includes 2 data points from an experiment with coins – 1 × one pence coin (diameter 20 mm) and 2 × two pence coins (diameter 26 mm) at AC 500 Hz.

Images they are poorly representative of a Gaussian curve. The coins and ball bearings are also different type geometries, the bearings being 3D and the coins closer to 2D objects. Assuming that FWHM can be applied to both bronze coins and steel ball-bearings, there is a first indication that the resolving limit for this system is around 20 mm, in agreement with our conclusions based on the images of different arrangements of two and six ball-bearings.

The 6.34 mm diameter ball-bearing gave the closest resemblance to a Gaussian curve for all three frequencies with maximum phase-differences of 0.25°, 0.2°, 0.16° for 20 kHz, 10 kHz, 5 kHz respectively. The 1D plots of 3.17 mm and 2.77 mm diameter ball-bearings, at each of the frequencies, except 3.17 mm at 20 kHz, gave a maximum phase difference of 0.01°, which is the smallest change in phase detectable by the lock-in amplifier. The FWHM for these plots was taken to be the width of the 0.01° rise in phase difference with respect to the corresponding length on the *y* axis.

It was noticed that depending on the size of the object, a different driver-coil frequency produced better results. For example; our measurements showed that small metallic-objects, down to the size of a 2.77 mm
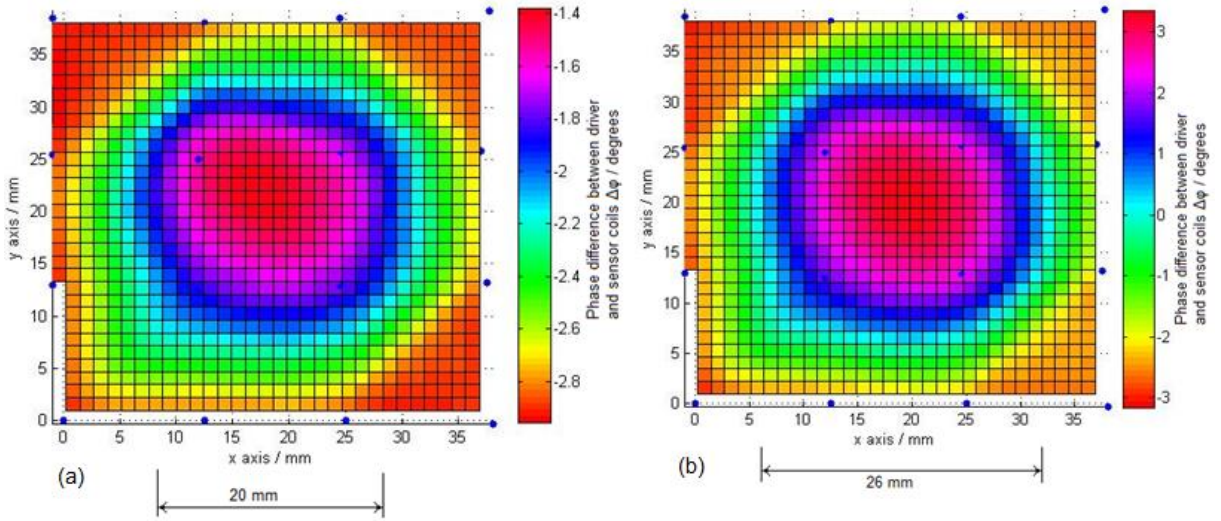
Fig. 5. (a) 2D surface plot showing phase difference Δφ, w.r.t. *x-y* position of a single one pence coin, with 4 × 4 sensor array underneath the sample object (sample is in between driver and sensor coils). The blue spots on the plot are the positions of the centre point of each sensor. Diameter of one pence coin = 20 mm. (a) The same as in (b) but imaging 2 × two pence coins, stacked directly on top of each other. Diameter of two pence coin = 26 mm.

Diameter steel ball-bearings, can be imaged by this MIT system, providing the frequency is high enough, in this case 5 kHz or above. It was discovered, from experimentation with the small ball bearings, that they image better at higher frequencies i.e. 10 kHz – 100 kHz. It was noted that the 6.34 mm diameter ball-bearing gave poor image quality at 500 Hz compared with 10 kHz.

3.3 Imaging two ball bearings through a ferromagnetic shield

An interesting issue is whether MIT can be used to image metallic objects through a metal screen. Clearly, such a possibility depends on many parameters; the size and the material of the object in the enclosure; the thickness and material of the enclosure; and the frequency of the driving field.

Presented here are the preliminary results for a small sample of different configurations. Firstly, a configuration of two 6.34 mm diameter ball-bearings with centres separated by 3 cm (figure 6a), 2 cm (figure 6b) and 1 cm (figure 6c).

The 2D plots of fig. 6 show the ball bearings imaged through a ferromagnetic shield of thickness 0.2 mm and height 1.5 cm in the red plots, and unshielded in the blue plots. The shielded (red plots) have 31 V (RMS) at   5 kHz applied across the driver coil. This is because at lower frequency and higher AC p.d. there is more penetration through the metallic shield. This is due to the skin depth [12-13] where:

$$\delta = \sqrt{\frac{2}{\omega\mu\sigma}} ,$$

(1)

which gives the depth at which the alternating magnetic-field has been attenuated to 37 % of its surface value, due to propagating through the material. Here $\omega = 2\pi f$ is the angular frequency; μ is the permeability of the metal shield and σ its conductivity. However, the frequency has to be large enough to produce a noticeable phase difference in the ball bearings, therefore 5 kHz was chosen. In the unshielded (blue) plots, the ball bearings are imaged in exactly the same positions, but at 10 kHz and 27 V (RMS) applied across the driver coil. Above 31 V (RMS) across the driver coil the sinusoidal AC signal in the sensor coil becomes distorted when imaging through
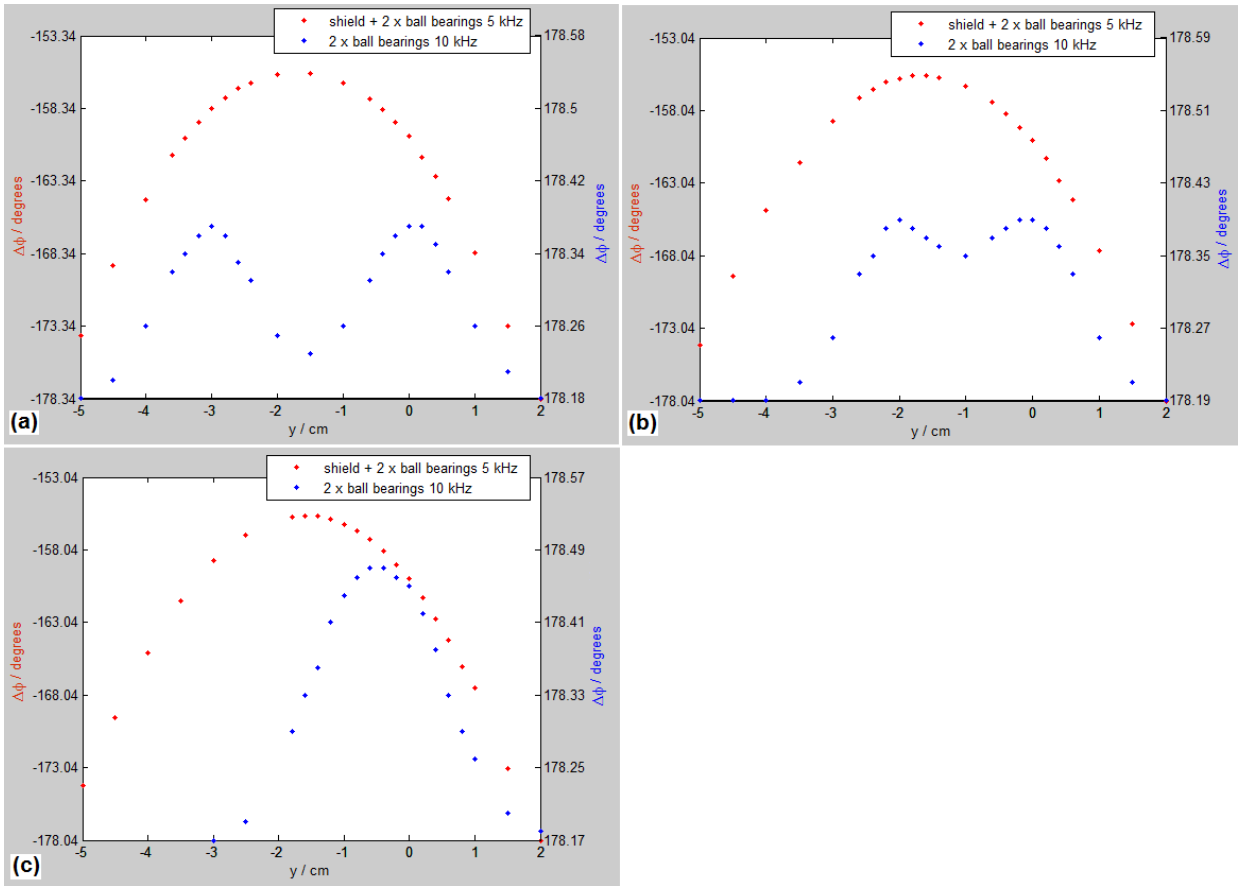
Fig. 6. For the red plots (with caption on the left): 1D plots of p.d. phase-difference, Δφ, along the *y* axis of 2 × 6.34 mm diameter ball bearings shielded by a ferromagnetic lid of thickness 0.2 mm and height 1.5 cm. An AC p.d. = 31 V (RMS) at 5 kHz was applied across the driver coil. The centres of the two ball bearings are separated by (a) 3 cm, (b) 2 cm and (c) 1 cm. The position of the ferromagnetic shield with respect to the plot is: -5.5 cm to +2 cm in the *y* axis and -3.7 cm to +4 cm in the *x* axis. The blue plots (with caption on the right) show the ball bearings in the same positions but unshielded and AC p.d. = 27.0 V (RMS) at 10 kHz across the driver coil.

The ferromagnetic shield. It was also found that the ball bearings gave largest phase-differences at ~27 V (RMS) across the driver coil, when the frequency was set to 10 kHz and so this was used in most of the experiments.

It can be seen from these three figures (6a, 6b and 6c), that no distortion in the curve of the red plots were observed to indicate the presence of the ball bearings, when attempting to image them through a ferromagnetic shield of thickness 0.2 mm. It can be seen from the red plots of figures 6a, 6b, and 6c that the p.d. phase-differences due to the presence of the shield is much larger than for the ball bearings, whose effect is dwarfed in comparison. As a result there is negligible detection of the ball bearings in these images.

In figures 6 and 7, the shielded phase-difference data is at 5 kHz, and the ball bearings on their own are at 10 kHz. Although this is not the most ideal comparison, they are not too dissimilar, as the maximum phase-difference (above the background phase) for a 6.34 mm diameter ball-bearing at 5 kHz is 0.16° and at 10 kHz it is 0.2°, with 27 V applied across the driver coil in both cases.

3.4 Imaging two ball bearings through an Aluminium foil shield

As a next step, the imaging of ball bearings was attempted through a thinner shield. In this case, a shield consisting of Aluminium foil was investigated. Figure 7 (a, b, c) show 1D images of two ball bearings with 3 cm, 2 cm and 1 cm separations between their centres, with the images being taken through a shield of

Aluminium foil of thickness 0.013 mm and height 1.6 cm, held in place by a wooden frame. The blue plots are the 6.34 mm diameter ball bearings imaged without the shield at 10 kHz with 27 V (RMS) applied across the driver coil. In the red plots the ball bearings are imaged through the Aluminium shield at 5 kHz with 31 V (RMS) applied across the driver
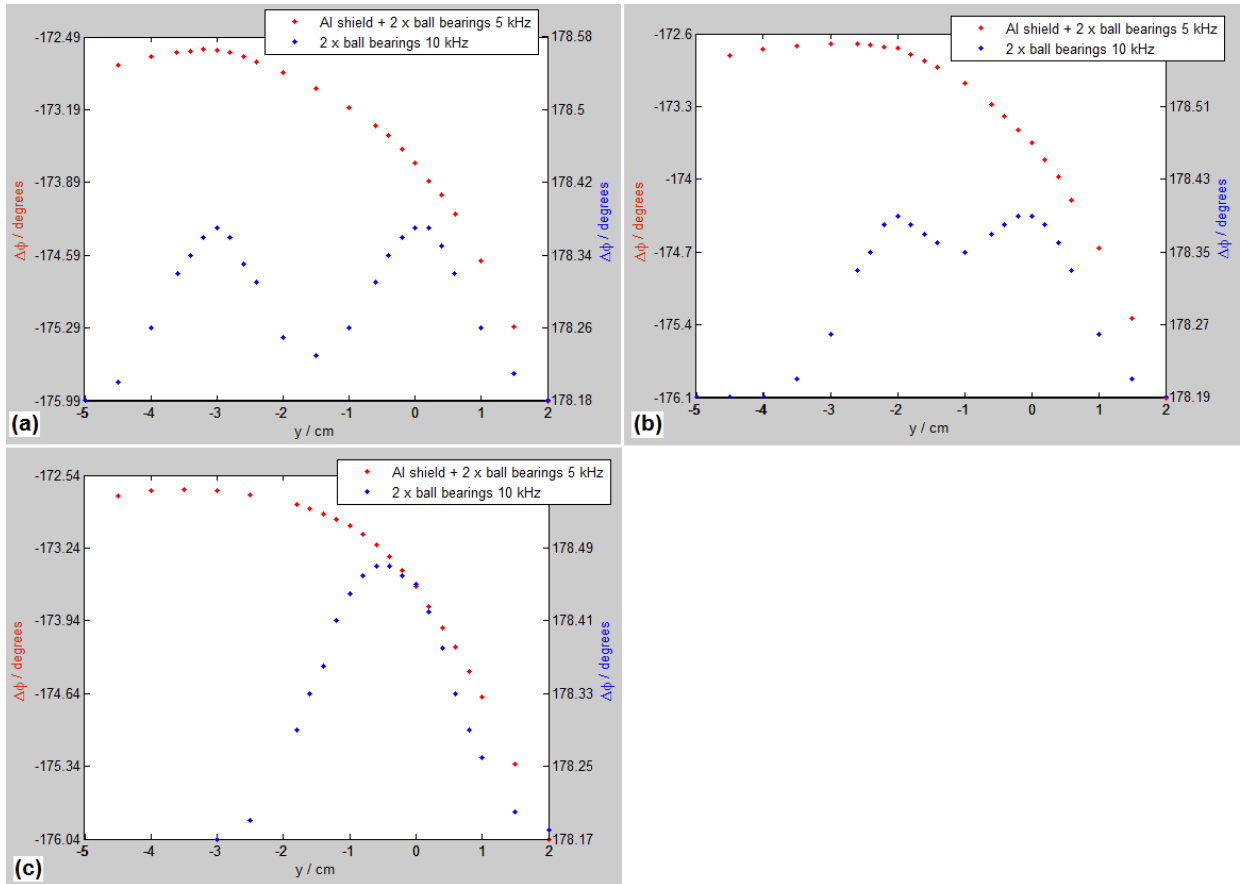

Fig. 7. 1D plots of p.d. phase-difference, $\Delta\varphi$, for 2×6.34 mm diameter ball bearings positioned along the y axis and imaged through an Aluminium (Al) foil shield of thickness 0.013 mm and height 1.6 cm. The ball bearings have their centres separated by: (a) 3 cm (b) 2 cm and (c) 1 cm. The plots show both shielded (red plots with caption on the left) and unshielded (blue plots with caption on the right). For shielded (red plots): AC p.d. across driver coil = 31 V (RMS) at 5 kHz. For unshielded (blue plots): AC p.d. across driver coil = 27 V (RMS) at 10 kHz.

The position of the shield with respect to the above plots is: -10.6 cm to +3.45 cm in the y axis and -4.5 cm to +5 cm in the x axis.

Coil. In comparing these three figures, it can be seen that the shielded images (red) change shape slightly between each plot, in relation to the position of the ball bearings, shown as slight rises in the curve. In figure 7a this is at $y = -3$ cm and $y = 0$ cm, in figure 7b at $y = -2$ cm and $y = 0$ cm, and in figure 7c at $y = -0.5$ cm. This result shows that steel ball-bearings of 6.34 mm diameter appear to be imaged through an Aluminium shield. Although it is not a decisive result, as the changes in the shielded images could be due to the delicate Aluminium foil changing shape slightly as it was removed and placed back again in between experiments.

3.5 Imaging a mild-steel bar through a ferromagnetic shield

Detecting ≤ 6.34 mm diameter steel ball bearings through a metallic shield involves testing this MIT system to its limits, as these sample objects are on the smallest end of the scale of what can be imaged. The 6.34 mm diameter ball-bearing requires high frequencies to obtain a satisfactory image i.e. 10 kHz and above. A more decisive result would be to image a larger metallic-object through a metal shield. This is described next and shown in the results of figure 8, imaging a mild-steel bar through the same ferromagnetic shield described earlier. In figure 8 the red plot shows the results of a 1D image of a mild-steel bar of width 2.6 cm, and thickness 2.29 mm, imaged through the ferromagnetic shield of length 7.45 cm and thickness 0.2 mm. The black plot shows an image of the mild-steel bar on its own, and the blue plot is the ferromagnetic shield on its own. In comparison, the red plot (steel bar + shield) shows considerably higher phase-difference than the blue plot (shield only). This is a clear result of the steel bar being imaged through a ferromagnetic shield.
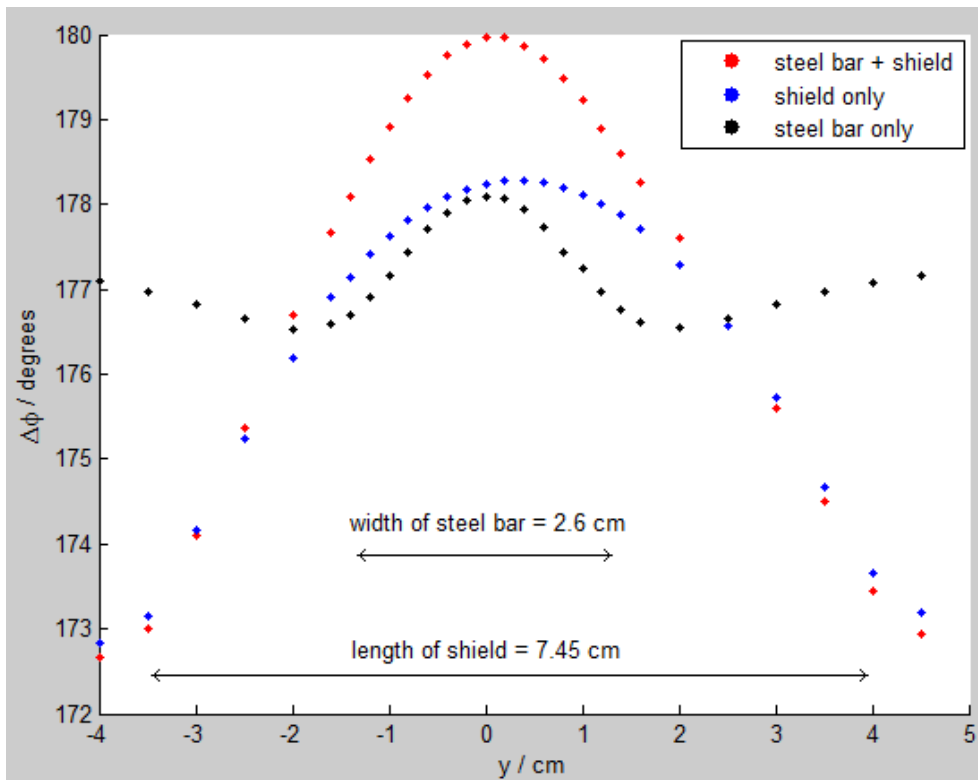

Fig. 8. 1D image plot of p.d. phase-difference, Δφ, along the *y* axis for a mild-steel bar imaged through a ferromagnetic shield (red plot); the ferromagnetic shield imaged on its own (blue plot); and steel bar imaged on its own (black plot). For this experiment the AC p.d. across the driver coil = 27.2 V (RMS) at 500 Hz.

4. Conclusion

In this study, a set of metallic objects (ball bearings and coins) have been used to explore the imaging capabilities of a simple MIT system based on a commercially available sensor-coil. The resolving power of the MIT system was estimated by using two different procedures. First, different arrangements of ball bearings were imaged, separated by different distances, and the minimum distance at which two ball-bearings could be resolved was determined. Second, the diameter of different ball-bearings and coins by using the FWHM of the MIT image was measured. The resolution of the system was then determined as the minimum diameter of the object for which the MIT measurement would give an appropriate value. The two procedures were found to give the same results, with a resolving power of about 20 mm.

The possibility of imaging metallic objects through ferromagnetic shields was also explored. Initial experiments with two ball-bearings imaged through ferromagnetic shields of thickness 0.2 mm gave negative results, with the signal due to the ball bearings being dwarfed in comparison with that of the shield, so that any effect was negligible and could not be determined from visual examination of the MIT images. The same experiment repeated with an Aluminium-foil shield showed slight rises in the curve where the ball bearings were placed. It was unclear whether the slight rises in the curve were due to the ball bearings themselves or a disturbance in the shape of the Aluminium foil when it was removed in-between experiments. This would need further investigation to determine any real effect. Finally a mild-steel bar was successfully imaged through a ferromagnetic shield using a low frequency (500 Hz) driving field. This seems to validate the possibility to image larger metallic samples through a ferromagnetic shield, provided they are not so large that they block the magnetic fields from reaching the sensor coil due to the skin effect.

Further work will involve the use of a 20 × 20 array of sensor coils, with an MIT system automated using computer-controlled multiplexers. This would be towards making MIT systems that are practical for security, industry or medicine. Larger AC magnetic fields will also be worked with, for deeper penetration through metal shields.

Acknowledgements

References

[1] Al-Zeibak S, Saunders, NH. A feasibility study of in vivo electromagnetic imaging. Physics in Medicine & Biology 1993, 38(1), pp. 151–160.
[2] Peyton AJ, Yu ZZ, Lyon G, Al-Zeibak S, Ferreira J, Velez J, Linhares F, Borges AR, Xiong HL, Saunders NH, Beck MS. An overview of electromagnetic inductance tomography: description of three different systems. Measurement Science and Technology, 1996, 7, pp. 261–271.
[3] Korjenevsky AV, Cherepenin VA. Progress in Realization of Magnetic Induction Tomography. *Ann NY Acad Sci* 1999, 873, pp. 346–352.
[4] Griffiths H, Stewart WR, Gough W. Magnetic Induction Tomography: A Measuring System for Biological Tissues. *Ann NY Acad Sci* 1999, 873, pp. 335–345.
[5] Griffiths H. Magnetic induction tomography. Measurement Science and Technology, 2001, 12, pp. 1126–1131.
[6] Griffiths H, Gough W, Watson S, Williams RJ. Residual capacitive coupling and the measurement of permittivity in magnetic induction tomography, Physiological Measurement, 2007, 28, pp. 301–311.
[7] Soleimani M. Simultaneous Reconstruction of Permeability and Conductivity in Magnetic Induction Tomography. *J Electromagnet Wave* 2009, 23, pp. 785–798.
[8] Zolgharni M, Griffiths H, Ledger PD. Frequency-difference MIT imaging of cerebral haemorrhage with a hemispherical coil array: numerical modelling. Physiological Measuremen,t 2010, 31, pp. 111–125.
[9] Wei H-Y, Soleimani M. A Magnetic Induction Tomography System for Prospective Industrial Processing Applications. The Chinese Journal of Chemical Engineering, 2012, 20(2), pp. 406–410.
[10] Wei H-Y, Ma L, Soleimani M. Volumetric magnetic induction tomography. Measurement Science and Technology, 2012, 23, pp. 1–9.
[11] Korjenevsky AV, Cherepenin VA, Sapetsky S. Magnetic induction tomography: experimental realization. Physiological Measurement, 2000;21:89–91.
[12] Gyselinck J, Vandevelde L, Melkebeek J, Dular P, Henrotte F, Legros W. Calculation of Eddy Currents and Associated Losses in Electrical Steel Laminations. *IEEE T Magn* 1999, 35(3) , p. 1192.
[13] Wheeler HA. Formulas for the Skin Effect. *P IRE* 1942, 30(9), p. 415.